PERGAMON

International Journal of Solids and Structures 40 (2003) 633–648

INTERNATIONAL JOURNAL OF SOLIDS and STRUCTURES

www.elsevier.com/locate/ijsolstr

Significance of distortion in thin-walled closed beam section design

Seok Heo [a], Jin Hong Kim [b], Yoon Young Kim [a,*]

[a] *School of Mechanical and Aerospace Engineering, Seoul National University Shinlim-Dong, San 56-1, Kwanak-Gu, Seoul 151-742, South Korea*

[b] *Vehicle Development and Analysis Team, Research and Development Division for Hyundai Motor Company and Kia Motors Corporation, 772-1, Changduk-Dong, Hwaseong-Si, Kyonggi-Do 445-706, South Korea*

Received 28 March 2002; received in revised form 19 September 2002

Abstract

Torsional and/or bending rigidities have been used as the key performance measure in conventional beam section design practice. The goal of this investigation is, however, to show that a so-called distortional rigidity also affects significantly the section shapes especially in the design of thin-walled closed beam sections. Though several investigations have analyzed complicated deformations of thin-walled beams such as distortion and warping, this paper is perhaps the first report to show how the design of thin-walled beam section shapes is affected by the additional consideration of the distortional rigidity. To illustrate this, several beam section optimization problems are considered.

Keywords: Thin-walled closed beam; Distortional rigidity; Torsional rigidity

1. Introduction

Most researches on beam section design have been focus on the maximization of torsional and bending rigidities (Banichuk and Karihaloo, 1976; Banichuk, 1976; Dems, 1980; Hou and Chen, 1985; Kim and Kim, 2000b; Mota Soares et al., 1984; Parbery and Karihaloo, 1980; Schramm and Pilkey, 1993; Schramm et al., 1995). Many of practically important beam sections have been successfully optimized with these rigidities. However, the section design considering torsional and/or bending rigidities alone often yields trivial section shapes especially when thin-walled *closed* sections are concerned. For example, the torsional rigidity maximization of a thin-walled closed section yields a square section if sections are restricted to remain quadrilateral.

In designing section shapes of thin-walled closed beams, it is worth noting that torsional and bending deformations are usually coupled with warping and distortional deformations that can affect significantly

* Corresponding author. Tel.: +82-2-880-7154; fax: +82-2-883-1513.
E-mail address: yykim@snu.ac.kr (Y.Y. Kim).

0020-7683/02/$ - see front matter
PII: S0020-7683(02)00617-0

the structural resistance of a beam. Because of the physical significance of warping and distortional deformations in thin-walled closed beams, many investigations are dedicated for the analysis of these deformations (Boswell and Zhang, 1984; Hsu et al., 1995; Kim and Kim, 1999, 2000a, 2001; Kim et al., 2002; Tesar, 1998; Wright et al., 1968). Pavazza (2002) has recently investigated the load distribution problem in thin-walled beams subjected to bending with respect to the cross-section distribution.

In spite of rich literature on the theory and analysis of these deformations, attempts to consider these deformations in section design are rare; Kim and Kim (2002) have recently considered the topology optimization of a beam under torsion and distortion. Though no notion of a distortional rigidity was introduced in Kim and Kim (2002), the importance of the distortional deformation was addressed in finding the optimal position of walls inside thin-walled closed sections.

The objective of this paper is to show that the design of thin-walled beam sections may be significantly affected by the additional consideration of a so-called distortional rigidity. To this end, we introduce the notion of a distortional rigidity and give its precise definition based on a higher-order thin-walled closed beam theory developed by Kim and Kim (1999, 2000a, 2001) To show the effect of the distortional rigidity on the optimized section shape, we construct a composite-objective function considering both the torsional and distortional rigidities. The optimized sections obtained with the composite-objective function are compared with those obtained with a single objective function considering only the torsional rigidity. Since the mean bending rigidity is always greater or equal to the torsional rigidity, only the torsional rigidity will be considered.

In Section 2, we review a thin-walled closed beams theory (Kim and Kim, 1999, 2000a, 2001) handling coupled deformations of torsion, warping and distortion. Based on this theory, we define the distortional rigidity in Section 3 by considering the limiting case of dominant distortional deformation. In Section 4, several case studies are investigated in the shape optimization framework of closed beam sections. This section will be following by conclusion.

2. Thin-walled closed beam theory

A one-dimensional theory of thin-walled closed beams for quadrilateral cross sections will be briefly given (see Kim and Kim, 1999, 2000a for more details). Fig. 1 shows the geometry of a quadrilateral thin-walled beam. The tangential coordinate s is measured along the contour of the cross section, and different origins are used for each wall. The normal coordinate n directs outwards from the contour. The displacements of a point on the middle line of the wall are expressed in terms of the normal u_n, tangential u_s and axial u_z components. The wall thickness is assumed to be constant.

If beam deformation measures are represented by the amounts of axial rotation $\theta(z)$, torsional warping $U^\theta(z)$, distortion $\chi(z)$ and distortional warping $U^\chi(z)$, the shell displacements are written as:

$$\begin{aligned} u_s(s,z) &= \psi_s^\theta(s)\theta(z) + \psi_s^\chi(s)\chi(z) \\ u_n(s,z) &= \psi_n^\theta(s)\theta(z) + \psi_n^\chi(s)\chi(z) \\ u_z(s,z) &= \psi_z^{U^\theta}(s)U^\theta(z) + \psi_z^{U^\chi}(s)U^\chi(z) \end{aligned} \tag{1}$$

where $\psi(s)$ are the functions of s describing the section deformations of the middle line of a thin-walled beam cross section in the n–s plane per unit value of θ, U^θ, χ and U^χ.

The section deformation associated with $\theta(z)$ is simply written as

$$\psi_s^\theta(s) = r(s) \quad \psi_n^\theta(s) = -l_i + s_i \tag{2}$$

where $r(s)$ is the normal distance from the shear center O to the tangent of a point on the contour, and l_i denotes the distance from the origin of the s_i coordinate on the ith wall to the point N_i (see Fig. 1).

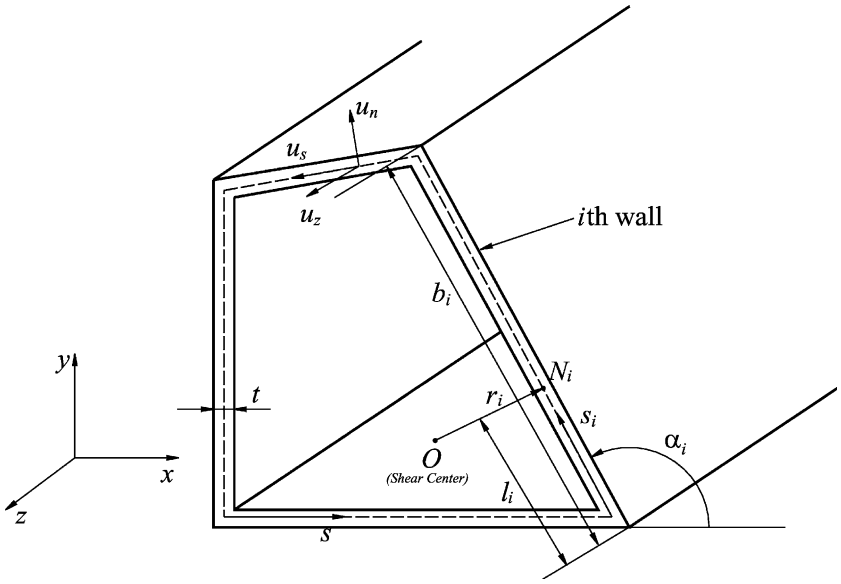

Fig. 1. Geometry of a quadrilateral thin-walled beam.

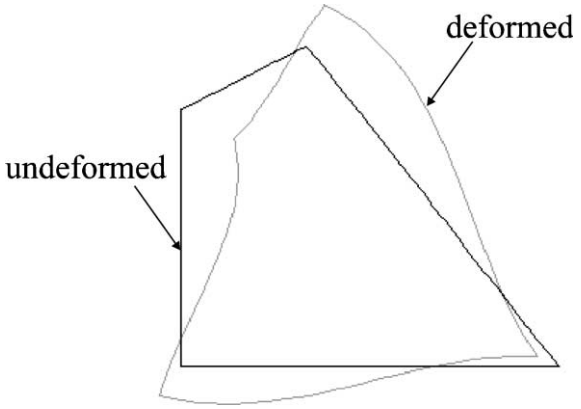

Fig. 2. Distortional shape of the centerline of a quadrilateral cross section.

The procedure to determine the tangential (ψ_s^χ) and normal (ψ_n^χ) displacements in components of the middle line corresponding to distortion $\chi(z)$ is not so straightforward for general quadrilateral sections. Instead of giving the detailed analytic procedure (which can be found in Kim and Kim, 1999), we merely illustrate a distortional deformation of a general quadrilateral section in Fig. 2.

For warping, there are two warping deformations associated with torsion and distortion, [1] which are usually referred to as a torsional and distortional warping. The torsional warping function is written as

[1] To simplify analysis, torsional and distortional warping deformations in quadrilateral sections may be assumed identical as in Kim and Kim (1999).

$$\psi_z^{U^\theta}(s) = \int (r_n - r)\,\mathrm{d}s + \psi_{z0}^{U^\theta} \tag{3}$$

where r_n is defined as $r_n = (\oint r\,\mathrm{d}s/\oint \mathrm{d}s) = (2\overline{A}/\oint \mathrm{d}s)$ with $\overline{A}$, the area enclosed by the beam cross section. The constant ψ_{z0}^{U} is determined from the condition that the average axial displacement of the torsional warping must vanish.

Similarly, the distortional warping function is given as

$$\psi_z^{U^\chi}(s) = \int \left[\psi_s^\chi(s) - \bar{\psi}_s^\chi\right]\mathrm{d}s + \psi_{z0}^{U^\chi} \tag{4}$$

where $\bar{\psi}_s^\chi$ is defined as $\bar{\psi}_s^\chi = (\oint \psi_s^\chi(s)\,\mathrm{d}s/\oint \mathrm{d}s)$ and $\psi_{z0}^{U^\chi}$ is also determined from the vanishing condition of the average axial displacement of the distortional warping.

Using the shell displacements expressed by Eq. (1), non-vanishing three-dimensional strains can be found. Using the resulting strains, the potential energy Π may be obtained

$$\Pi = \frac{1}{2}\int \sigma_{ij}\epsilon_{ij}\,\mathrm{d}V - \int (pu_z + qu_s)\,\mathrm{d}V + \Pi_\mathrm{b} \tag{5}$$

where p and q denote external axial and tangential forces, respectively and Π_b represents the potential due to Neumann-type boundary conditions. Integrating Eq. (5) over the the beam cross-section A, we can obtain the following one-dimensional form of the system potential energy:

$$\begin{aligned}\Pi = \frac{1}{2}\int &\left[M_z\theta' + Q\chi' + B_{U^\theta}U^{\theta'} + B_{U^\chi}U^{\chi'} + \overline{B}_{U^\theta}U^\theta + \overline{B}_{U^\chi}U^\chi + \overline{Q}\chi\right]\mathrm{d}z \\ &- \int (p_1U^\theta + p_2U^\chi + q_1\theta + q_2\chi)\,\mathrm{d}z + \Pi_\mathrm{b}\end{aligned} \tag{6}$$

In Eq. (6), $(\ )'$ implies the differentiation with respect to z and p_1, p_2, q_1 and q_2 are one dimensional load terms. The definitions of M_z etc. are

$$\begin{aligned}
M_z &\equiv G[b_2U^\theta + b_8U^\chi + b_1^*\theta' + b_4\chi'] \\
Q &\equiv G[b_3U^\theta + b_9U^\chi + b_4\theta' + b_5\chi'] \\
B_{U^\theta} &\equiv E_1[a_1U^{\theta'} + a_2U^{\chi'}] \\
B_{U^\chi} &\equiv E_1[a_2U^{\theta'} + a_3U^{\chi'}] \\
\overline{B}_{U^\theta} &\equiv G[b_1U^\theta + b_7U^\chi + b_2\theta' + b_3\chi'] \\
\overline{B}_{U^\chi} &\equiv G[b_7U^\theta + b_6U^\chi + b_8\theta' + b_9\chi'] \\
\overline{Q} &\equiv E_1c\chi
\end{aligned} \tag{7}$$

where $E_1 = E(1-\nu^2)$. Note that E, G and ν are Young's, shear modulus and Poisson's ratio.

The coefficients introduced in Eq. (7) are defined as

$$
\begin{aligned}
&a_1 = \int_A \left(\psi_z^{U^\theta}\right)^2 \mathrm{d}A, \quad a_2 = \int_A \psi_z^{U^\theta}\psi_z^{U^\chi}\,\mathrm{d}A, \quad a_3 = \int_A \left(\psi_z^{U^\chi}\right)^2 \mathrm{d}A \\
&b_1^* = \int_A \left(\psi_s^\theta\right)^2 \mathrm{d}A, \quad b_1 = \int_A \left(\frac{\mathrm{d}\psi_z^{U^\theta}}{\mathrm{d}s}\right)^2 \mathrm{d}A, \quad b_2 = \int_A \psi_s^\theta \frac{\mathrm{d}\psi_z^{U^\theta}}{\mathrm{d}s}\,\mathrm{d}A \\
&b_3 = \int_A \psi_s^\chi \frac{\mathrm{d}\psi_z^{U^\theta}}{\mathrm{d}s}\,\mathrm{d}A, \quad b_4 = \int_A \psi_s^\theta\psi_s^\chi\,\mathrm{d}A, \quad b_5 = \int_A \left(\psi_s^\chi\right)^2 \mathrm{d}A \\
&b_6 = \int_A \left(\frac{\mathrm{d}\psi_z^{U^\chi}}{\mathrm{d}s}\right)^2 \mathrm{d}A, \quad b_7 = \int_A \frac{\mathrm{d}\psi_z^{U^\theta}}{\mathrm{d}s}\frac{\mathrm{d}\psi_z^{U^\chi}}{\mathrm{d}s}\,\mathrm{d}A, \quad b_8 = \int_A \psi_s^\theta \frac{\mathrm{d}\psi_z^{U^\chi}}{\mathrm{d}s}\,\mathrm{d}A \\
&b_9 = \int_A \psi_s^\chi \frac{\mathrm{d}\psi_z^{U^\chi}}{\mathrm{d}s}\,\mathrm{d}A, \quad c = \int_A n^2 \left(\frac{\mathrm{d}^2\psi_n^\chi}{\mathrm{d}s^2}\right)^2 \mathrm{d}A
\end{aligned}
\tag{8}
$$

The coefficients b_1 and b_2 are related as $b_2 = -b_1$.

3. Distortional rigidity of thin-walled closed beams

In this section, we propose the notion of a distortional rigidity. As the distortional rigidity has some analogy with the torsional rigidity, we begin our discussion with the torsional rigidity. Although the torsional rigidity is well known, the understanding of the procedure to derive the torsional rigidity from the theory given in Section 2 is important to understand the distortional rigidity.

When neglecting the in-plane distortion χ and the associated warping U^χ, the total potential energy in Eq. (6) can be expressed in terms of rotation θ and torsional warping U^θ:

$$
\Pi = \frac{1}{2}\int \left[M_z\theta' + B_{U^\theta}U^{\theta'} + \overline{B}_{U^\theta}U^\theta\right]\mathrm{d}z - \int \left(p_1U^\theta + q_1\theta\right)\mathrm{d}z + \Pi_\mathrm{b} \tag{9}
$$

where

$$
\begin{aligned}
&M_z = G[b_2U^\theta + b_1^*\theta'] = G[-b_1U^\theta + b_1^*\theta'] \\
&B_{U^\theta} = E_1a_1U^{\theta'} \\
&\overline{B}_{U^\theta} = G[b_1U^\theta + b_2\theta'] = G[b_1U^\theta - b_1\theta']
\end{aligned}
\tag{10}
$$

In Eq. (10), we used $b_2 = -b_1$. If we consider the case of $U^\theta = \theta'$ (this condition is used for uniform torsion problems), Eq. (10) becomes

$$
M_z = G[b_1^* - b_1]\theta' = C_\mathrm{t}\theta' \tag{11}
$$

From Eq. (11), the torsional rigidity C_t is identified as $G(b_1^* - b_1)$. Note that $G(b_1^* - b_1)$ reduces to the well-known expression of the torsional rigidity of thin-walled closed beams

$$
G(b_1^* - b_1) = \frac{4Gt\overline{A}^2}{\oint \mathrm{d}s} \tag{12}
$$

To introduce the distortional rigidity, it is convenient to consider the case where the rotation θ and the rotational warping U^θ vanish. In this case, the total potential energy (6) reduces to

$$
\Pi = \frac{1}{2}\int \left[Q\chi' + BU^{\chi'} + \overline{B}U^\chi + \overline{Q}\chi\right]\mathrm{d}z - \int \left(p_2U^\chi + q_2\chi\right)\mathrm{d}z + \Pi_\mathrm{b} \tag{13}
$$

where

$$\begin{aligned} Q &= G[b_9 U^{\chi} + b_5 \chi'] \\ B_{U^{\chi}} &= E_1 a_3 U^{\chi'} \\ \overline{B}_{U^{\chi}} &= G[b_6 U^{\chi} + b_9 \chi'] \\ \overline{Q} &= E_1 c \chi \end{aligned} \tag{14}$$

Following the procedure used to derive the relation $b_2 = -b_1$, we find that

$$b_9 = -b_6 \tag{15}$$

In the case of $U^{\chi} = \chi'$ (similar to $U^{\theta} = \theta'$ for torsion), the following equilibrium equation is obtained (Eq. (15) is used):

$$E_1 a_3 \chi'''' - Gb\chi'' + E_1 c\chi = p_{\mathrm{ex}} \tag{16}$$

where $b = b_5 - b_6$ and p_{ex} denotes the external load. This equation is similar to the governing equation for beams on elastic foundations (BEF) in which $E_1 c$ is equivalent to the elastic foundation stiffness. Boswell and Zhang (1984) and Tesar (1998) derived a similar equation for distortion problems. Wright et al. (1968) and Hsu et al. (1995) addressed the usefulness of the analogy between this distortion problem and the BEF problem.

In the limiting case of the uniform distortion ($\chi' = 0$), the only stiffness of the beam is due to $E_1 c$. Consequently we propose to define the distortional rigidity D as

$$D = E_1 c = E_1 \int_A n^2 \left(\frac{\mathrm{d}^2 \psi_n^{\chi}}{\mathrm{d}s^2} \right)^2 \mathrm{d}A \tag{17}$$

Referring to Eq. (16), one can see that the distortional rigidity D is the main rigidity against uniform distortion.

4. Effects of distortional rigidity

In this section, closed beam section optimization problems are setup in order to illustrate the effects of the distortional rigidity in design of beam sections. First, we deal with section optimization in single-cell cross sections and then in multi-cell cross sections. The importance of the distortional rigidity may be best revealed in section design optimization.

4.1. Single-cell cross section

We first consider the significance of the distortional rigidity in single-cell cross sections. The mathematical statement of beam section optimization problems can be given as:

Minimize

$$f = -w_c \log C_{\mathrm{t}} - w_d \log D \tag{18}$$

Subject to

$$\left(\sum_{i=1}^{N} b_i \right) - L_{\mathrm{c}} = 0 \tag{19}$$

In Eq. (18), w_c and w_d are factors adjusting relative weightings between C_t and D. Since the torsional rigidity C_t is always smaller than the mean bending rigidity (see, e.g., Kim and Kim, 2002), no bending rigidity is considered explicitly in the objective function (18). The torsional rigidity for thin-walled closed beams is defined in Eq. (12).

Eq. (19) represents the beam mass constraint where L_c is the total length of the beam centerline. Assuming that all walls have the same thickness, the prescribed total wall length L_c is equivalent to the total mass density of a beam. The coordinates (x_i, y_i) of the ith corner of a beam section are used as design variables, and each wall length b_i is subject to side constraints,

$$b_l < b_i < b_u \quad (i = 1, \ldots, n_e) \tag{20}$$

where b_l and b_u are the lower and upper bounds of b_i, respectively and n_e is the total number of edges. For all design problems considered in this work, the modified feasible direction method (Vanderplaats, 1999) is employed. Since the present investigation is mainly concerned with the investigation of the effects of the distortional rigidity, no effort is made to carry out the analytic sensitivity analysis. Instead, we simply take a straightforward finite difference scheme, where $\partial f/\partial x_i$ and $\partial f/\partial y_i$ are replaced by $\Delta f/\Delta x_i$ and $\Delta f/\Delta y_i$ with $\Delta x_i = \Delta y_i = 0.01$.

When the distortional rigidity is not considered, the conventional objective function only considering the torsional rigidity is considered.

$$f_1 = -C_t, \quad \text{or} \quad f_1 = -\log C_t \tag{21}$$

The advantage of using the logarithmic function was reported in Kim and Kim (2002).

Example 1 (*Quadrilateral section design*)**.** As the first problem, we consider the design optimization of a quadrilateral beam section in Fig. 3. The numerical data for the present problem are

$$L_c = 40 \text{ mm}, \quad w_c = 0.002, \quad w_d = 0.0031, \quad b_l = 0 \text{ mm}, \quad b_u = 40 \text{ mm}$$

An additional constraint that a beam section remains symmetric with respect to the y-axis is also imposed.

Figs. 4(a) and (b) show the optimized cross section shapes with f_1 and f, respectively. If we consider only the torsional rigidity for optimization, the resulting section becomes square as anticipated. This result is obvious because a circular cross section has the largest torsional rigidity and the result shown in Fig. 4(a) is the quadrilateral section closest to a circular section. However, the optimized section in Fig. 4(b) obtained

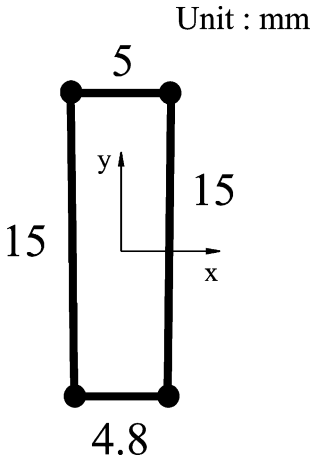

Fig. 3. A rectangular single-cell section ($E = 2.068 \times 10^{11}$ N/m^2, $G = 8.019 \times 10^{10}$ N/m^2, $t = 1$ mm).

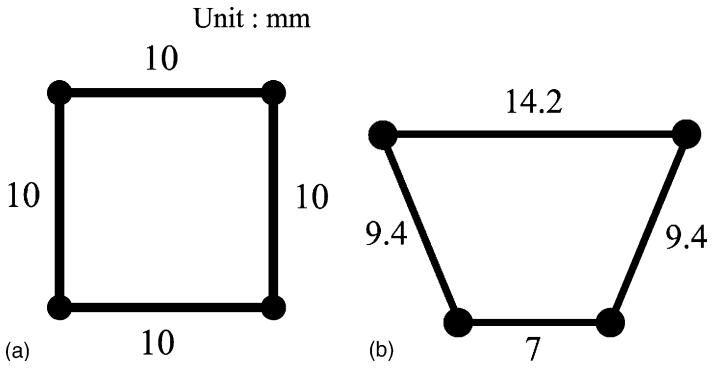

Fig. 4. Optimized section shapes using (a) f_1 for torsional rigidity maximization and (b) f for balanced torsional and distortional rigidity maximization.

by considering both torsional and distortional rigidities is a trapezoidal section. This result shows that a trapezoidal section has a larger resistance to section distortion than a rectangular section, and this is why trapezoidal sections are common in bridge construction.

Fig. 5 shows the history of the composite-objective function f as well as the history of the corresponding torsional and distortional rigidities. It is worth examining the structural performance of the present trapezoidal section over a square section under a couple of the same magnitude applied at one end of the thin-walled beam (see Fig. 6). The maximum shear and axial stresses in both beams are calculated using plate finite elements provided by I-DEAS (I-DEAS, 1993). For this problem, $E = 2.068 \times 10^{11}$ N/m^2, $G = 8.019 \times 10^{10}$ N/m^2 and the density of $\rho = 7820$ kg/m^3 are used. Table 1 shows the effectiveness of the trapezoidal section over the square section. In addition to the stress analyses, free-vibration analyses for the two beams having free ends are carried out. The lowest three eigenfrequencies are compared in Table 2. For reference, Fig. 7 shows the first two eigenmodes of the square box beam, which are dominated by distortional deformations.

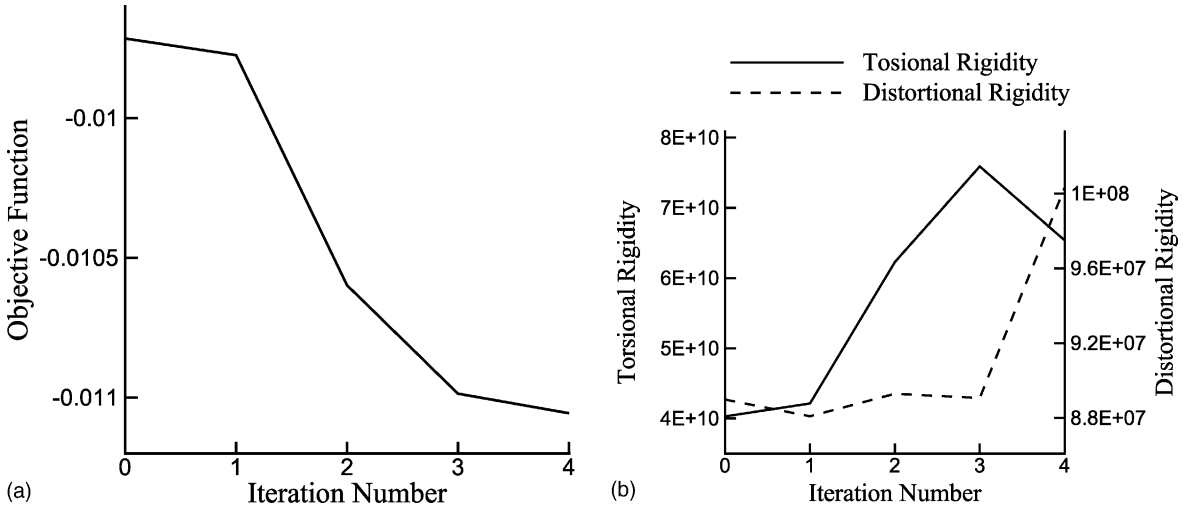

Fig. 5. (a) The history of the objective function f and (b) the histories of the corresponding torsional and distortional rigidities for a single-cell section shown in Fig. 4(b).

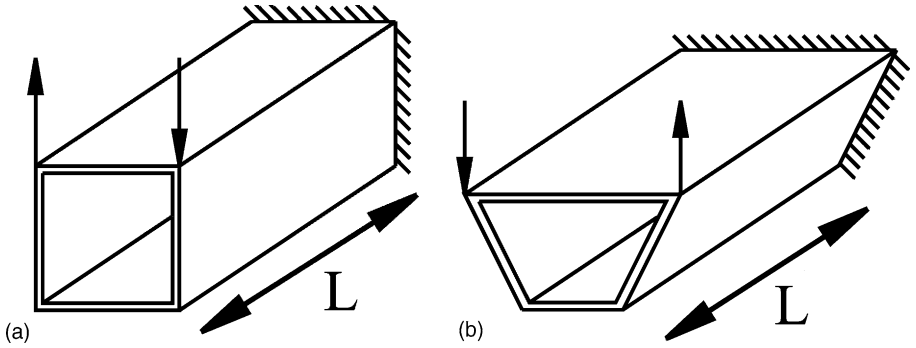

Fig. 6. Cantilevered box beams having (a) a square and (b) a trapezoidal section under a couple having the same magnitude $M = 1.0 \times 10^{-5}$ N m ($L = 50$ mm).

Table 1
Maximum shear stress τ_{max} and axial stress $(\sigma_z)_{max}$ (unit: N/m^2)

Section type	τ_{max}	$(\sigma_z)_{max}$
Square (Fig. 6(a))	282.0	287
Trapezoid (Fig. 6(b))	256.0	124

Table 2
Eigenfrequencies of square and trapezoidal box beams

Section	Distortional mode 1	Distortional mode 2	Torsional mode
Square (Fig. 6(a))	1.40 kHz	1.42 kHz	2.75 kHz
Trapezoid (Fig. 6(b))	1.65 kHz	1.62 kHz	2.60 kHz

The results given in Tables 1 and 2 show that the consideration of the distortional rigidity affects significantly the section design. Unless applied loads induce pure torsional (or bending) deformation in beams, the consideration of the distortional rigidity can improve quite substantially the structural performance of thin-walled closed beams.

Example 2 (*General section design*)**.** As the next example, a thin-walled section shown in Fig. 8(a) is optimized for $L_c = 40$ mm in Eq. (18). The design optimization using f ($w_c = 1$, $w_d = 2.5$) and f_1 will be studied. The optimized designs based on f_1 and f are shown in Fig. 8(a) and (b), respectively. The histories of the objective function, the torsional and distortional rigidities for Fig. 8(c) are plotted in Fig. 9.

This example reveals the significant effects of the distortional deformations in the section shape optimization. In Fig. 10, the present section shape obtained in Fig. 8(c) is compared with a center-pillar section of a typical passenger car. Since two sections in Fig. 10 have a similar section configuration, it can be deduced that pillar sections in automobiles can effectively resist against sectional distortion. For this problem, it may be worth investigating the effects of the weighting factors w_d on the optimized shapes. The results are shown in Fig. 11.

4.2. Multi-cell section design

In this subsection, the design of multi-cell sections considering the distortional rigidity is considered. To simplify discussions, we will be mainly focusing on double-cell quadrilateral sections, but the present approach can be extended to general multi-cell sections.

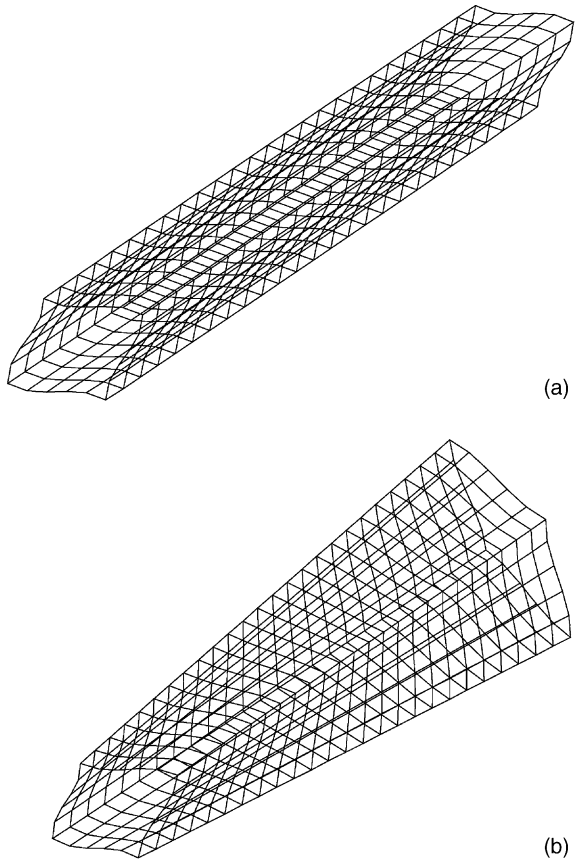

Fig. 7. (a) The first and (b) the second eigenmode of a square box beam with free ends.

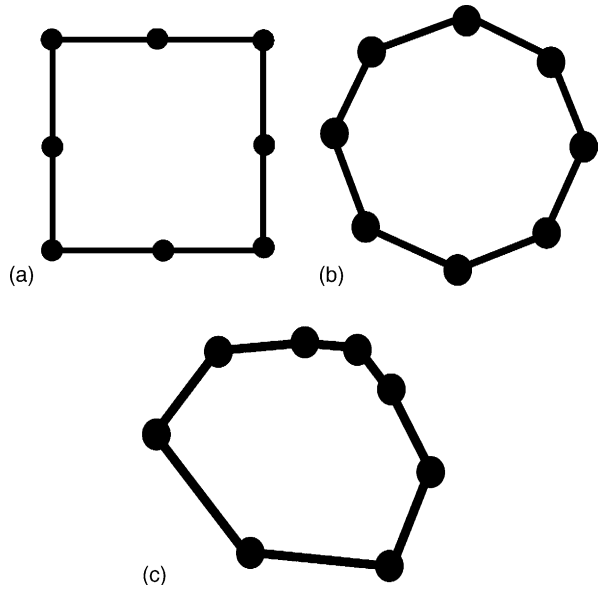

Fig. 8. A general thin-walled cross section (a) before optimization, (b) design optimization with f_1, and (c) with f.

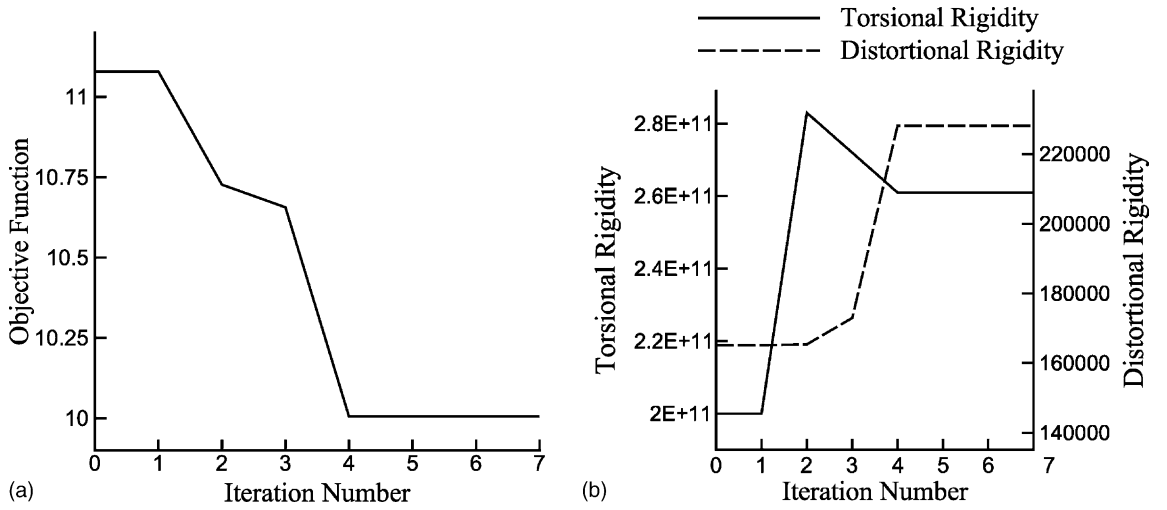

Fig. 9. (a) The history of the objective function f and (b) the histories of the corresponding torsional and distortional rigidities for a general thin-walled section shown in Fig. 8(c).

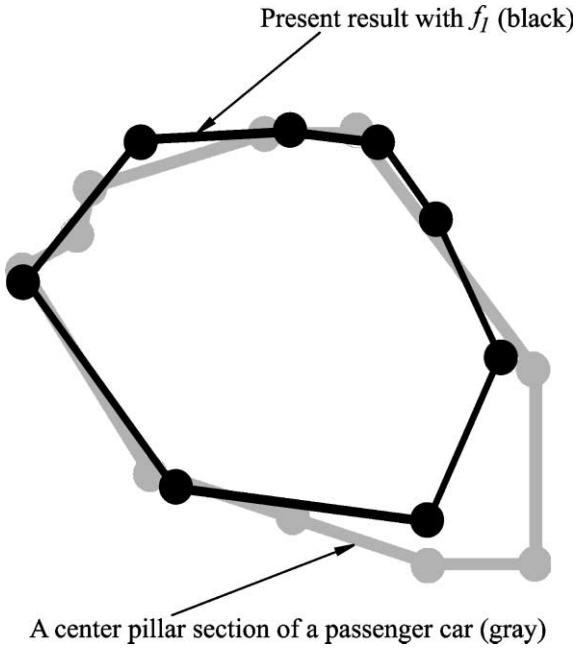

Fig. 10. The comparison of the present result (black) and a center pillar section of a typical pillar passenger car (gray).

The torsional rigidity C_t^m of a double-cell section shown in Fig. 12 can be found by using the following equations (see, e.g., Oden (1967)):

$$M_z = C_t^m \alpha^m = \sum_{i=1}^{2} 2q_i \overline{A}_i \tag{22}$$

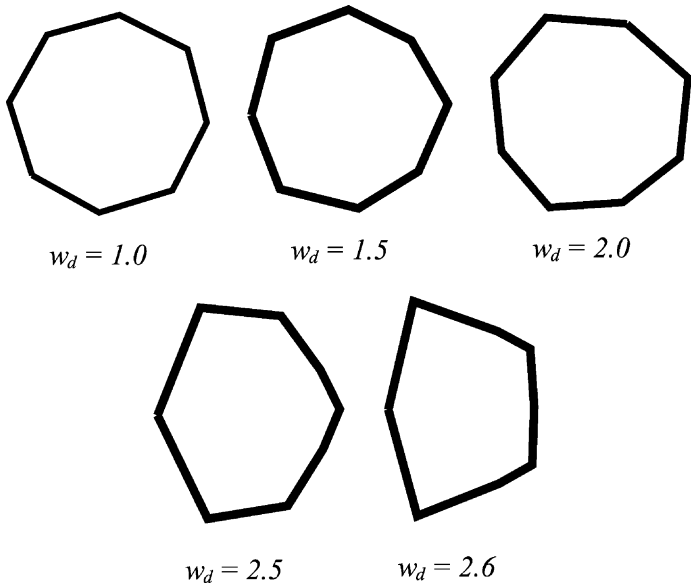

Fig. 11. The effects of the weighting factors w_d on the optimization section shapes (w_c in f is fixed as 1.0).

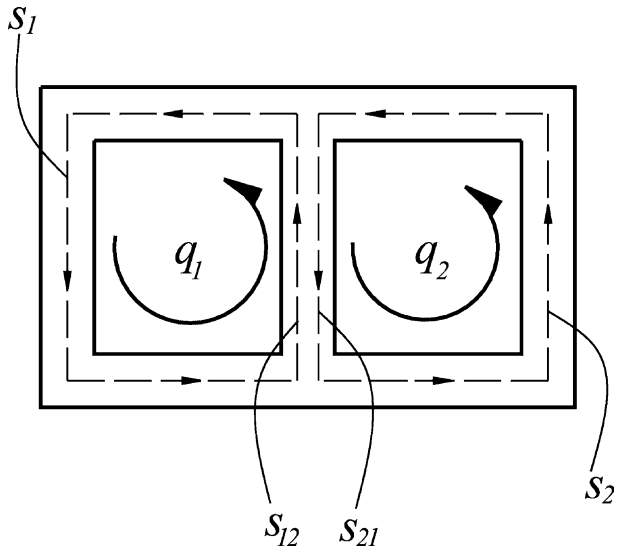

Fig. 12. A double-cell cross section.

$$\alpha^m = \frac{1}{2G\overline{A}_1}\left(q_1 \oint_{s_1} \mathrm{d}s/t - q_2 \int_{s_{12}} \mathrm{d}s/t\right) \tag{23}$$

$$\alpha^m = \frac{1}{2G\overline{A}_2}\left(q_2 \oint_{s_2} \mathrm{d}s/t - q_1 \int_{s_{21}} \mathrm{d}s/t\right) \tag{24}$$

where α^m is the twist per unit length and q_i and $\overline{A}_i$ denote the shear flow and the enclosed area of the ith cell, respectively. Eqs. (23) and (24) represent the condition of the single-valuedness of the axial displacement of the torsional warping in double cells. In Eqs. (23, 24), $\int_{s_i}$ denotes the contour integration around the ith cell and $\int_{s_{ij}}$ represents the integration along the wall common to the ith and jth cells. The positive direction of s_{ij} is designated in Fig. 12.

In determining the distortional rigidity of multi-cell sections, we should be aware of the existence of two distortional deformations in a double-cell quadrilateral section. (There is only one distortional mode in a single-cell quadrilateral section.) Kim and Kim (2001) have recently presented a step-by-step procedure to determine distortional deformation shapes for multi cells. Following the procedure given in Kim and Kim (2001), two distortional deformation modes shown in Fig. 13(a) are obtained. One may also find the distortional rigidities for a double-cell section by extending the method used for a single-cell section.

Denoting the two distortional rigidities of a double-cell section by D_1^m and D_2^m, one may construct an objective function for multi-cell section optimization problems as

$$f^m = -w_t^m \log C_t^m - w_{d_1}^m \log D_1^m - w_{d_2}^m \log D_2^m \tag{25}$$

In this case, however, adjusting the relative ratio w_{d_1}/w_{d_2} of the weighting factors for the distortional rigidities is obscure. Based on this observation, we approximate each distortional deformation mode of the double-cell section as the combination of the distortional deformation of a single-cell section (see Fig. 13(b)). Since the total distortional rigidity of a multi-cell section is governed by the minimum rigidity between the distortional rigidities of two separate single cells, we propose to employ the following form of the objective function for multi-cell sections:

$$f^m = -w_t^m \log C_t^m - w_d^m \log D_{\min} \tag{26}$$

where

$$D_{\min} = \min(D_1, D_2) \tag{27}$$

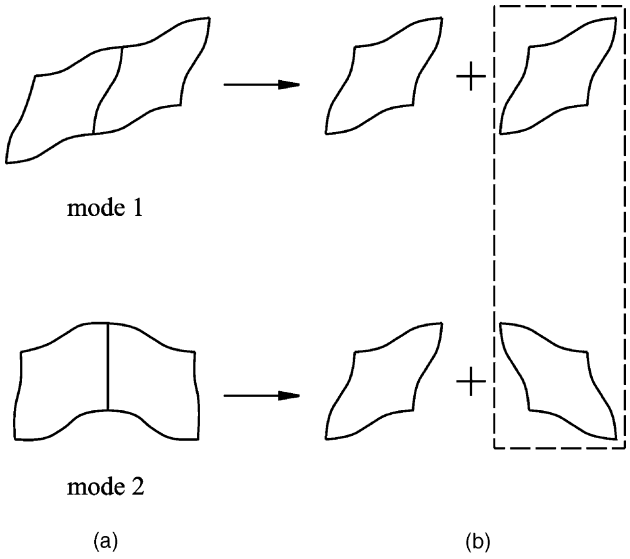

Fig. 13. (a) Two distortional modes of a double-cell cross section, and (b) decomposed modes into those of single cells.

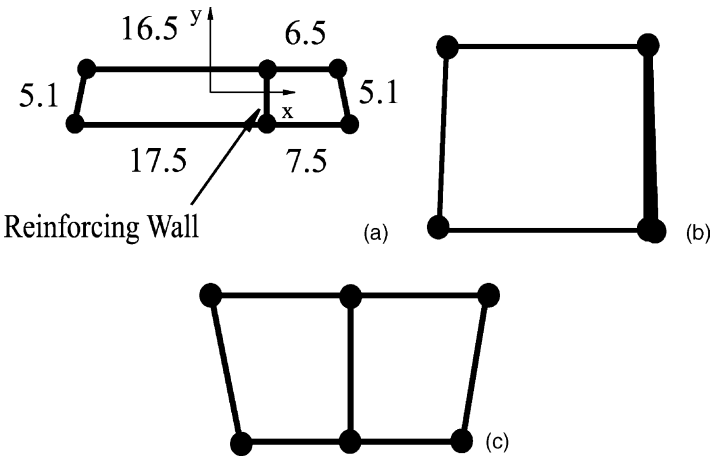

Fig. 14. A double-cell cross section (a) before optimization, (b) after the torsional rigidity maximization and (c) after the optimization to maximize the torsional and distortional rigidities ($w_c = 1.0$ and $w_d = 3.0$).

In Eq. (27), D_i denotes the distortional rigidity of the ith single cell defined as

$$D_i = E_1 c_i = E_1 \int_{A_i} n^2 \left(\frac{\mathrm{d}^2 \psi_{ni}^{\chi}}{\mathrm{d}s^2} \right)^2 \mathrm{d}A \tag{28}$$

The performance of f^m in Eq. (26) will be compared with that with the conventional objective function f_1 given by Eq. (21).

Example 3 (*Double-cell quadrilateral section design*)**.** A double-cell section design problem shown in Fig. 14(a) will be considered as an example. In this case, we are interested in finding the optimal location of the reinforcing wall in symmetric cross sections.

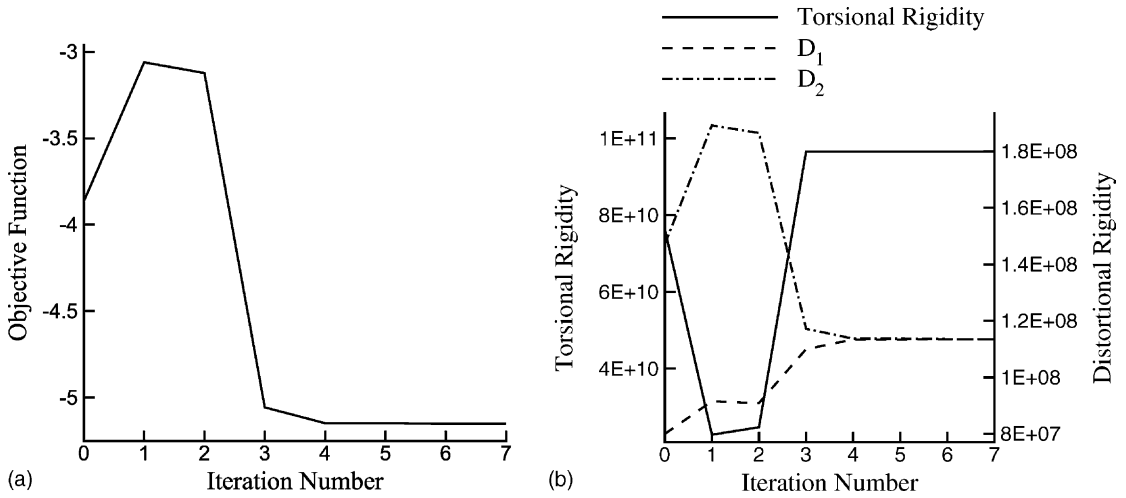

Fig. 15. (a) The history of the objective function f^m and (b) the histories of the corresponding torsional and distortional rigidities for the design depicted in Fig. 14(c).

The value L_c for the constraint equation (19) is set to be 55 mm. If f_1 in Eq. (21) is used as the objective function, the resulting beam section becomes a single-cell section as shown in Fig. 14(b); the reinforcing wall is merely pushed to a side member. This result is trivial as the design optimization using the torsional rigidity alone does not provide any practically useful information.

However, the section optimization using the composite-objective function f^m considering both the torsional and distortional rigidities yields a satisfactory result as shown in Fig. 14(c). The reinforcing wall in Fig. 14(c) does not help increase the torsional rigidity, but the distortional rigidity. Fig. 15 shows the history of the objective function f^m and the histories of the corresponding torsional and distortional rigidities. Note that the section shown in Fig. 14(c) is indeed a section used in wide bridges. This problem also exemplifies the significant effects of the distortional rigidity in thin-walled closed beam section design. The use of a composite-objective function consisting of torsional and distortional rigidities in practical applications is expected to provide very useful design information.

5. Conclusion

Starting from a higher-order thin-walled closed beam theory, a notion of the distortional rigidity is introduced. The significant effects of the distortional rigidity in the design of thin-walled closed beam sections have been revealed by several case studies. In the course of this investigation, a new composite-objective function considering both the torsional and distortional rigidities for multi-cell sections is also proposed.

Acknowledgement

This work was supported by the Brain Korea 21 (BK21) Project.

References

Banichuk, N.V., 1976. Optimization of elastic bars in torsion. International Journal of Solids and Structures 12, 275–286.

Banichuk, N.V., Karihaloo, B.L., 1976. Minimum-weight design of multi-purpose cylindrical bars. International Journal of Solids and Structures 12, 267–273.

Boswell, L.F., Zhang, S.H., 1984. The effect of distortion in thin-walled box-spine beams. International Journal of Solids and Structures 20 (9/10), 845–862.

Dems, K., 1980. Multiparameter shape optimization of elastic bars in torsion. International Journal for Numerical Methods in Engineering 15, 1517–1539.

Hou, J.W., Chen, J.L., 1985. Shape optimization of elastic hollow bars. ASME Journal of Mechanisms, Transmissions, and Automation in Design 107, 100–105.

Hsu, Y.T., Fu, C.C., Schelling, D.R., 1995. EBEF method for distortional analysis of steel box girder bridges. Journal of Structural Engineering 121 (3), 557–566.

I-DEAS, FEM User's Guide. 1993. Structural Dynamics Research Corporation, SDRC, Milford.

Kim, J.H., Kim, Y.Y., 1999. Analysis of thin-walled closed beams with general quadrilateral cross sections. ASME Journal of Applied Mechanics 66 (4), 904–912.

Kim, J.H., Kim, Y.Y., 2000a. One-dimensional analysis of thin-walled closed beams having general cross-sections. International Journal for Numerical Methods in Engineering 49, 653–668.

Kim, Y.Y., Kim, T.S., 2000b. Topology optimization of beam cross section. International Journal of Solids and Structures 37, 477–493.

Kim, J.H., Kim, Y.Y., 2001. Thin-walled multi-cell beam analysis for coupled torsion, distortion and warping deformation. ASME Journal of Applied Mechanics 68, 260–269.

Kim, T.S., Kim, Y.Y., 2002. Multi-objective topology optimization of a beam under torsion and distortion. AIAA Journal 40 (2), 376–381.

Kim, J.H., Kim, H.S., Kim, D.W., Kim, Y.Y., 2002. New accurate efficient modeling techniques for the vibration analysis of T-joint thin-walled box structures. International Journal of Solids and Structures 39, 2893–2909.

Mota Soares, C.A., Rodrigues, H.C., Oliveira Faria, L.M., Haug, E.J., 1984. Optimization of the geometry of shafts using boundary elements. ASME Journal of Mechanisms, Transmissions, and Automation in Design 106, 199–202.

Pavazza, R., 2002. On the load distribution of thin-walled beams subjected to bending with respect to the cross-section distortion. International Journal of Mechanical Sciences 44, 423–442.

Parbery, R.D., Karihaloo, B.L., 1980. Minimum-weight design of thin-walled cylinders subject to flexural and torsional stiffness constraints. ASME Journal of Applied Mechanics 47, 106–110.

Oden, J.T., 1967. Mechanics of Elastic Structure. McGraw-Hill Book Company.

Schramm, U., Pilkey, W.D., 1993. Structural shape optimization for the torsion problem using direct integration and B-splines. Computer Methods in Applied Mechanics and Engineering 107, 251–268.

Schramm, U., Pilkey, W.D., DeVries, R.I., Zebrowski, M.P., 1995. Shape design for thin-walled beam cross sections using rational B splines. AIAA Journal 33 (11), 2205–2211.

Tesar, A., 1998. The effect of diaphragms on distortion vibration of thin-walled box beams. Computers and Structures 66 (4), 499–507.

Vanderplaats, G.N., 1999. Numerical Optimization Techniques for Engineering Design, third ed. Colorado Springs.

Wright, R.N., Abdel-Samad, S.R., Robinson, A.R., 1968. BEF analogy for analysis of box girders. Journal of the Structural Division, Proceeding of the American Society of Civil Engineers 94 (7), 1719–1743.